A Climatological View of the Kuroshio/Oyashio System East of Japan*

TANGDONG QU

International Pacific Research Center, SOEST, University of Hawaii, Honolulu, Hawaii

HUMIO MITSUDERA

Frontier Research System for Global Change, Tokyo, Japan and International Pacific Research Center, SOEST, University of Hawaii, Honolulu, Hawaii

BO QIU

Department of Oceanography, SOEST, University of Hawaii, Honolulu, Hawaii

(Manuscript received 8 May 2000, in final form 11 December 2000)

ABSTRACT

Time-averaged structure of the Kuroshio/Oyashio system east of Japan was examined using historical hydrographic data. Unlike most of the earlier climatological analyses, the data were averaged along isopycnal rather than pressure surfaces in a 0.5° × 0.5° grid. As a result, most of the detailed phenomena associated with the narrow western boundary currents were revealed. Water from the Oyashio is seen to overshoot the zero zonally integrated wind-stress-curl line by more than 5°, approaching as far south as 36°–38°N at the western boundary. Water from the Kuroshio Extension, by contrast, tends to feed into the Oyashio Front in the interior ocean. This exchange of waters leads to a zero of zonally integrated (western boundary–180°) meridional transport at about 44°N, reasonably coinciding with the zero of zonally integrated wind stress curl in the western North Pacific. A well-defined double-front structure is seen at depths of the thermocline, but it does not appear to have a strong signature in the surface dynamic topography. Though always accompanied by strong temperature and salinity gradients, water density changes little across the Oyashio Front near the surface. Both the Kuroshio Extension and Oyashio Front have a significant deep component, but below 1000 m the former seems to be dominated by eddy features associated with the Kuroshio Extension recirculation gyre.

1. Introduction

The Kuroshio/Oyashio system (KOS) has captured the interest of oceanographers as well as fishermen for about a century because of the abundant fishery resource in the mixed water region (MWR) east of Japan (cf. Kawai 1972). Since the early 1990s, interest in the KOS has increased further due to the long-lasting negative excursion of the Southern Oscillation index, which among other things has been linked to the Pacific decadal variability (e.g., Nakamura et al. 1997; Miller et al. 1998; Xie et al. 2000). Hypotheses to account for this variability involve changes in the shallow, meridional circulation cells that allow exchange of waters between the main oceanic gyres, namely the subtropical and subpolar cells. The KOS is especially important in these cells because it is a crossroad of their prominent pathways (McCreary and Lu 1994; Lu et al. 1998).

Studies of the KOS have been fairly diverse, using hydrographic/XBT observations (e.g., Mizuno and White 1983; Joyce 1987; Talley 1993), direct current measurements (e.g., Schmitz et al. 1987; Joyce and Schmitz 1988), and satellite altimetry data (e.g., Qui et al. 1991; Qiu and Kelly 1993). There is no doubt that these studies were particularly useful because they provided the basis for understanding the KOS from various points of view. However, as most of them depended on synoptic analysis, the resulting descriptions of the KOS were time dependent. Although some of them used repeated sections along 152°E, 165°E, and 175°W, they were separated randomly in the zonal direction (e.g., Niiler et al. 1985; Joyce 1987; Schmitz and Niiler 1987; Joyce and Schmitz 1988). As a result, a three-dimensional, time-averaged picture of the KOS is still lacking. For many oceanographic applications, knowledge of the mean conditions is desirable, and this is particularly true for studies using satellite altimetry (Qiu 1995). By omit-

* School of Ocean and Earth Science and Technology Contribution Number 5300, and International Pacific Research Center Contribution Number IPRC-67.

Corresponding author address: Dr. Tangdong Qu, IPRC-SOEST, University of Hawaii, 2525 Correa Road, Honolulu, HI 96822.
E-mail: tangdong@soest.hawaii.edu

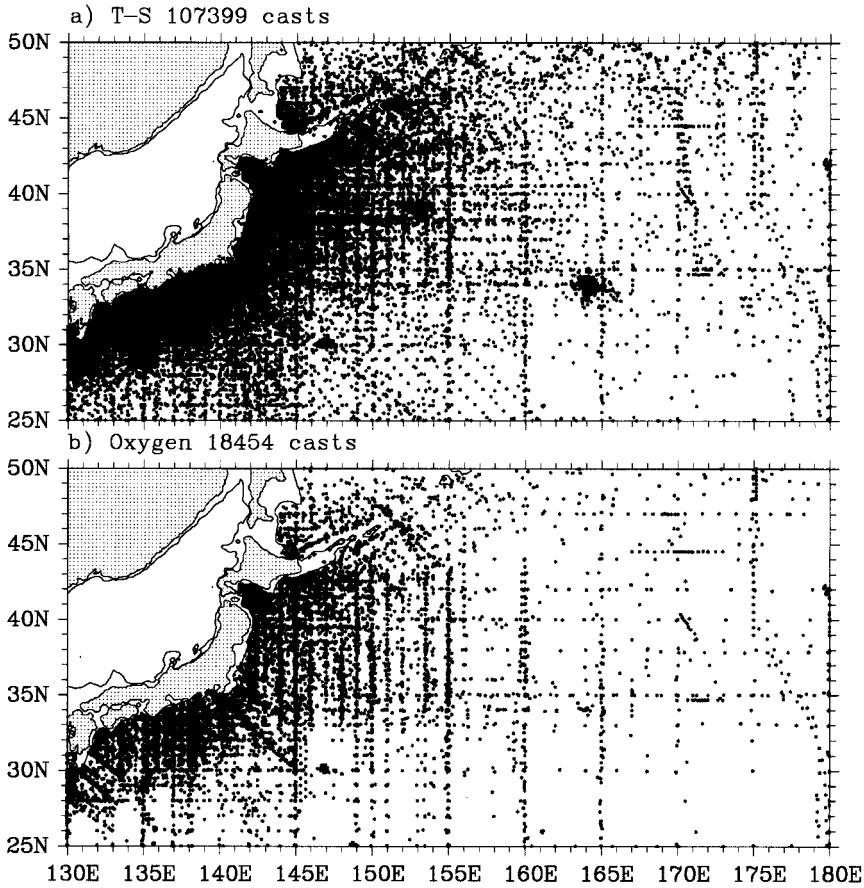

FIG. 1. Geographical distribution of stations (asterisk) of (a) temperature/salinity and (b) oxygen used for this study. Solid lines indicate 200-m isobath.

ting small-scale or transient features, and thereby emphasizing sustained signals otherwise hidden by turbulence, climatological analyses have proven to be an effective approach.

For the last 18 years or so, the most widely used observational source both for regional and global analyses has been the climatological atlas of Levitus (1982, 1994). As the objective analysis in preparing this atlas involves smoothing of more than 700 km, it fails to show many detailed phenomena associated with the narrow western boundary currents (Qu et al. 1998). Furthermore, this atlas was prepared by averaging along pressure surfaces. In the MWR, where isopycnals are strongly sloping, this procedure likely produces significant artificial smoothing of properties at depths of the pycnocline. To address this concern, Macdonald et al. (2001) recently prepared an isopycnally averaged North Pacific climatology. Despite some improvement as stated by its authors, the resolution ($1^\circ \times 1^\circ$) of this new dataset does not seem to be enough to resolve the KOS adequately.

In this study, we seek a climatological study of the KOS that differs from the earlier work of Levitus (1982, 1994) in that (i) data are averaged along isopycnal surfaces and (ii) a $0.5^\circ \times 0.5^\circ$ grid is used with *e*-folding smoothing scales less than 100 km. Based on all quality-controlled historical observations (Macdonald et al. 2001), we provide a zero-order description of the time-averaged flow in the western North Pacific. Oxygen data are also used as a passive tracer to provide independent information on the pathways of water masses. As will be seen, the new climatology includes many important small-scale semipermanent features and thus gives a more accurate picture of the KOS east of Japan.

The rest of the paper is arranged as follows. In section 2, we describe the data and methods of analysis used for this study. In section 3, we illustrate vertically integrated circulation. Sections 4 and 5 are devoted to showing upper-layer circulation on pressure and isopycnal surfaces, respectively. Sectional distributions of properties are shown in section 6, and middepth circulation is examined in section 7. Results are summarized in section 8.

2. Data and methods of analysis

For this study, the hydrobase format raw data (Macdonald et al. 2001) for the region 25°–50°N, 130°E–

180° were used. These include all the CTD and bottle profiles at observed levels that were not flagged as ''bad'' or as not passing the monthly, seasonal, and annual standard deviation checks with water depth greater than 200 m recorded on the CD-ROMs of World Ocean Database 1994. We further selected the data by the removal of profiles with obviously erroneous records both in location and measured values (e.g., those with temperature higher than 8°C below 1000 m or salinity lower than 30 psu below 100 m, and those incorrectly located on land). Interestingly, some profiles have extremely high density, exceeding 27.5 σ_θ before reaching 800 m depth. Since we could not tell whether these high-density profiles were real or not, we just eliminated them as erroneous records.

We abandoned all oxygen data obtained before 1956 (Suga and Hanawa 1990; Macdonald et al. 2001) and those with oxygen concentration less than 2 ml l^{-1} in the upper 200 m or greater than 10 ml l^{-1} below that depth. The geographic distribution of the final dataset used for this study, shown in Fig. 1, includes 107 399 profiles of temperature/salinity and 18 454 profiles of oxygen concentration. The spatial distribution of the data is basically the same for the four seasons (not shown), but there are nearly twice as many observations in summer (Jun–Aug) as in winter (Dec–Feb).

To limit the artificial smoothing of features in vertical obtained when averaging on pressure surfaces around the pycnocline, we first interpolate water properties at observed levels onto a set of density surfaces with a 0.02 kg m^{-3} vertical resolution using cubic spline and then perform the averaging in a 0.5° × 0.5° grid (Gouriou and Toole 1993). The number of samples at each grid is usually larger than 10 and can be as large as several hundreds near the coast of Japan. In some parts of the interior ocean, where data coverage is relatively sparse, we chose variable horizontal radius to include at least five samples for each grid. Close to the surface, the concept of averaging on isopycnal surfaces breaks down because of the outcropping of shallower isopycnals. Following Gouriou and Toole (1993), the average properties between the mean mixed layer base (defined as the first depth at which the potential density is 0.1 kg m^{-3} greater than the surface value) and the first isopycnal surface present on all profiles were obtained by linear interpolation (also see Qu et al. 1999). Then, the average properties are smoothed using Gaussian filter, with an *e*-folding scale of 75 km for temperature/salinity and 100 km for oxygen, considering their different sampling density, and interpolated back to a 10-dbar uniform pressure series in the upper 1000 m. Averaging is conducted simply along pressure surfaces at depths below 1000 m, with smoothing scales about twice as large as in the shallower waters. While deeper observations were available at some locations, the present study is restricted to the upper 2000 m to optimize uniformity of the database.

Standard deviations of properties (temperature, salinity, and oxygen concentration) also obtained during averaging are used to edit the mean fields. Observations that differ from the grid mean by more than three standard deviations are discarded. In addition, estimates of standard deviations are also used to measure the robustness of patterns on the property maps. The details are given in the appendix.

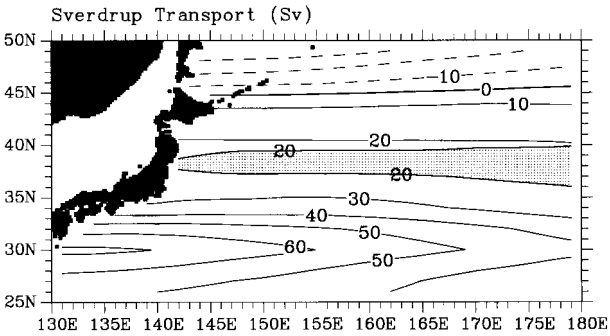

FIG. 2. Sverdrup transports (Sv) calculated from Hellerman and Rosenstein's (1983) wind stress. The shaded area indicates a local minimum (<20 Sv) of Sverdrup transport.

3. Vertically integrated circulation

a. Sverdrup transport

According to steady Sverdrup theory, the division between the subtropical and subpolar gyres should occur at the zero of barotropic, wind-driven Sverdrop transport defined as the zonally integrated wind stress curl to the eastern boundary. Hellerman and Rosenstein's (1983) annual mean wind stress curl indicates that this zero line is situated at about 45°N with a slight southward shift toward the west (Fig. 2). Eastward flow is seen in a broad latitude band from 30° to 43°N, and its volume transport exceeds 60 Sv (Sv $\equiv 10^6$ m^3 s^{-1}). More than half of this eastward flow seems to turn southwestward before reaching the international dateline, indicative of a large anticyclonic circulation associated with the subtropical gyre. The eastward flow to the north of 45°N constitutes the southern portion of the subpolar gyre.

By close inspection of Fig. 2, we found a local minimum <20 Sv of transport at 36°–40°N. In the sense of linear Sverdrup dynamics, this result implies that there should exist a weak westward flow between the Kuroshio Extension and Oyashio Front. We will return to this point in section 6.

b. Levitus climatology

Dynamic height *D* relative to 2000 dbar is calculated from the climatological temperature and salinity (Levitus 1994), and these values are then integrated from 2000 m to the sea surface to produce the transport function (called the depth-integrated dynamic height hereafter), that is, $P = g^{-1}\int_{2000\text{m}}^{0} D\, dz$. Given any two points

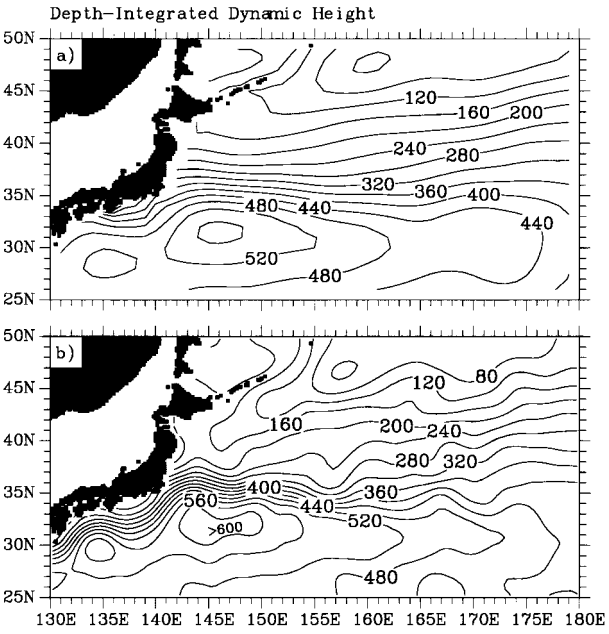

FIG. 3. Depth-integrated (0–2000 m) dynamic height (m²) relative to 2000 db, calculated from (a) the Levitus climatology and (b) the present data. Contour intervals are 40 m². The value of 1220 m² has been subtracted before plotting.

A and B, in the ocean, the volume transport between them is determined by

$$Q_{AB} = (P_A - P_B)g/f, \quad (1)$$

where g is the acceleration due to gravity, and f is the Coriolis parameter.

The depth-integrated dynamic height (Fig. 3a) shows essentially a similar pattern of circulation with Sverdrup transport (Fig. 2) in the interior ocean, and the division between the subtropical and subpolar gyres seems to be identical in the two figures. This suggests that, despite the presence of baroclinic processes, inertial effects, and locally wind-driven fluctuations Sverdrup theory still provides a useful picture of the large-scale horizontal gyres in the North Pacific. The largest discrepancies are seen near the western boundary where Sverdrup theory is not applicable and Levitus (1994) climatology is most problematic. In the subpolar gyre, the depth-integrated dynamic height demonstrates the presence of the Oyashio along the coast of the Kuril Islands, but the Sverdrup transport does not. In the subtropical gyre, however, both figures fail to give a meaningful picture of the Kuroshio. One obvious reason for this failure in Fig. 3a is due to heavy smoothing of properties along pressure surfaces, as already noted in section 1.

c. Present result

The Kuroshio, as a swift and narrow northeastward flow along the continental slope south of Japan, is well resolved in our new climatology (Fig. 3b). It makes a southward deflection at about 138°E, reflecting the Kuroshio path bimodality, and flows into the deep ocean in a meander path extending as far as 155°E. Downsteam of 160°E or so, the Kuroshio Extension transforms from a concentrated narrow current into the weak, broad North Pacific Current (Kawai 1972), where the transition excursions of the Kuroshio Extension observed from synoptic data (e.g., Mizuno and White 1983) appear as a diffusion in the mean path, presumably due to temporal smoothing in the multidecadal span.

Two anticyclonic meanders are present in the mean path of the Kuroshio Extension: one around 144°E and the other close to 150°E (Fig. 3b), and this meander pattern is similar to that detected by Kawai (1972) and Mizuno and White (1983). As has been argued (Hurlburt et al. 1996), bottom topography, that is, the sea mounts just east of the trench (143°–144°E) and the abyssal plain to the further east, may have strong influence on these meanders. Because of the conservation of potential vorticity, the abyssal currents forced by the baroclinic instability allow the bottom topography to steer the path of the Kuroshio Extension. Part of the Kuroshio Extension separates from its main stream at 155°–160°E and proceeds northeastward, presumably representing the observed bifurcation in the vicinity of Shatsky Rise around 158°E (Mizuno and White 1983; Qiu et al. 1991).

Also noted are changes in volume transport of the Kuroshio Extension along its flow path. According to Eq. (1), the relative mean transport (0–2000 dbar) of the Kuroshio Extension, defined as the eastward flow south of 38°N, is about 40 Sv around its separation point (140°E) and increases toward a maximum of approximately 51 Sv at 144°E. Downstream of that longitude the transport decreases gradually to about 41 Sv at 152°E and 33 Sv at 160°E. To the south of the main axis of the Kuroshio Extension, depth-integrated dynamic height drops by about 214 m² from 144° to 180°E. At 32°N, this indicates a recirculation of about 27 Sv [Eq. (1)]. These estimates of the Kuroshio Extension are smaller, compared with the earlier estimates of 57 Sv (Niiler et al. 1985) and 87 ± 21 Sv (Hall 1989) at 152°E and 56 ± 2 Sv at 165°E relative to the ocean bottom (Joyce 1987). The selection of a reference level (2000 dbar) might miss the deeper component of the Kuroshio Extension.

In contrast with Fig. 3a, the Oyashio is seen to extend as far south as 36°–38°N off Honshu. From there, much of it turns cyclonically toward the northeast before heading eastward along 40°–45°N. The relative mean transport (0–2000 dbar) of the Oyashio is about 16 Sv east of the Kuril Islands between 150° and 158°E at 47°N [Eq. (1)]. In the Oyashio Front, eastward transport has a maximum of about 17 Sv at 158°E, characterized by a drop of depth-integrated dynamic height of 177 m² from 40° to 47°N. Close to the international dateline, the broad eastward-flowing North Pacific Current (35°–50°N) carries about 33 Sv of mixed water into the central North Pacific.

The southward intrusion of the Oyashio, often defined by the isolines 5°C in temperature and/or 33.5 psu in salinity at depth 100 m, is already known (e.g., Kawai 1972; Sekine 1988). However, as subsurface temperature and salinity are strongly affected by local wind and surface heat flux, significant discrepancies have been reported among synoptic maps. Here we provide a time-averaged picture suggesting that this phenomenon is robust and extends to a greater depth than ever observed. Part of the water from the subpolar gyre overshoots the zero zonally integrated wind stress curl (Fig. 2) by more than 5° at the western boundary. In addition to the possible influence of bottom topography and coastal geometry (Hurlburt et al. 1996; Mitsudera et al. 1998), the southward intrusion of the Oyashio could also be interpreted as a result of large-scale interaction between the subtropical and subpolar gyres. For example, in the interior ocean, we see waters separating from the Kuroshio Extension and proceeding northeastward to feed into the Oyashio Front (Fig. 3b). This northward transfer of waters counterbalances most of the southward intrusion of the Oyashio and leads to a zero zonally integrated (western boundary–180°) meridional transport at about 44°N, reasonably coinciding with the zero zonally integrated wind stress curl (Fig. 2).

4. Shallow-depth circulation

Figure 4a illustrates the mean dynamic height distribution (relative to 2000 dbar) at the sea surface. Compared with its depth-integrated counterpart (Fig. 3b), surface dynamic topography exhibits a vague boundary between the Kuroshio Extension and Oyashio Front, suggesting that the double-front structure of the KOS does not have a strong signature at the sea surface. South of the Kuroshio Extension, surface dynamic topography contains several (four with the contour interval chosen) semiclosed contours, while its depth-integrated counterpart (Fig. 3b) is dominated by a completely closed large anticyclonic gyre often known as the Kuroshio Extension recirculation gyre (KERG) centered at 145°–150°E. Apparently, the latter reflects the contribution from the deeper-layer circulation. The semiclosed dynamic height contours at the sea surface, almost evenly distributed in the longitude band from 145°E to 180°, curve southeastward south of 25°N and join the shallow, eastward-flowing Subtropical Countercurrent (Nitani 1972; Qiu 1999).

The double-front structure of the KOS becomes well defined at depths of the thermocline. A region of homogenous dynamic height appears at depth 500 m (Fig. 4b) and is even more evident at 800 m (Fig. 4c) between the Kuroshio Extension and Oyashio Front west of 160°E. South of the Kuroshio Extension, maps of dynamic topography at these depths reveal the existence of a closed anticyclonic gyre, a phenomenon that is not seen at the sea surface.

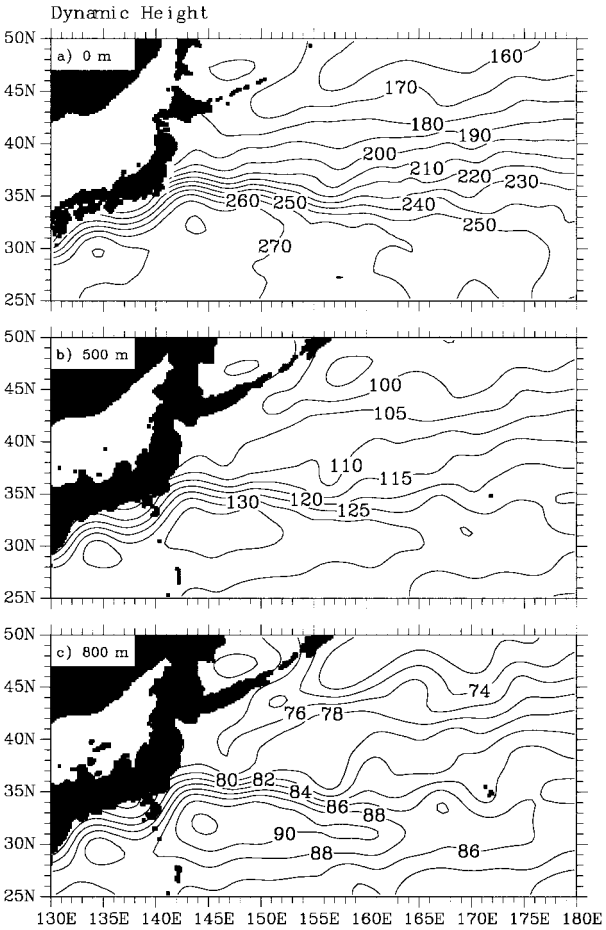

FIG. 4. Dynamic height (dyn cm) at (a) sea surface and depth (b) 500 m and 800 m relative to 2000 dbar. Contour intervals are 10 dyn cm for (a), 5 dyn cm for (b), and 2 dyn cm for (c).

5. Circulation and water mass distribution on isopycnal surfaces

Since water parcels are expected to flow along density surfaces, it is useful to look at property distributions on isopycnals. Three isopycnals, $\sigma_\theta = 26.2$, 26.8, and 27.2, are chosen to show the distributions of depth, potential temperature, salinity, oxygen concentration, potential vorticity, and acceleration potential.

a. $\sigma_\theta = 26.2$

The 26.2 σ_θ surface outcrops at 38°–40°N (dashed lines in Fig. 5) in winter (Levitus 1994). In the annual mean field, this density surface lies at depths ranging from less than 50 m in the subpolar region to more than 500 m in the dynamical center of the subtropical gyre (Fig. 5a). The depth variation suggests that the Kuroshio Extension is characterized by strong horizontal density gradients in the shallow waters, despite relatively uniform potential temperature and salinity ($\theta \sim 10.0$°C, $S \sim 34.2$ psu). This condition is just reversed in the

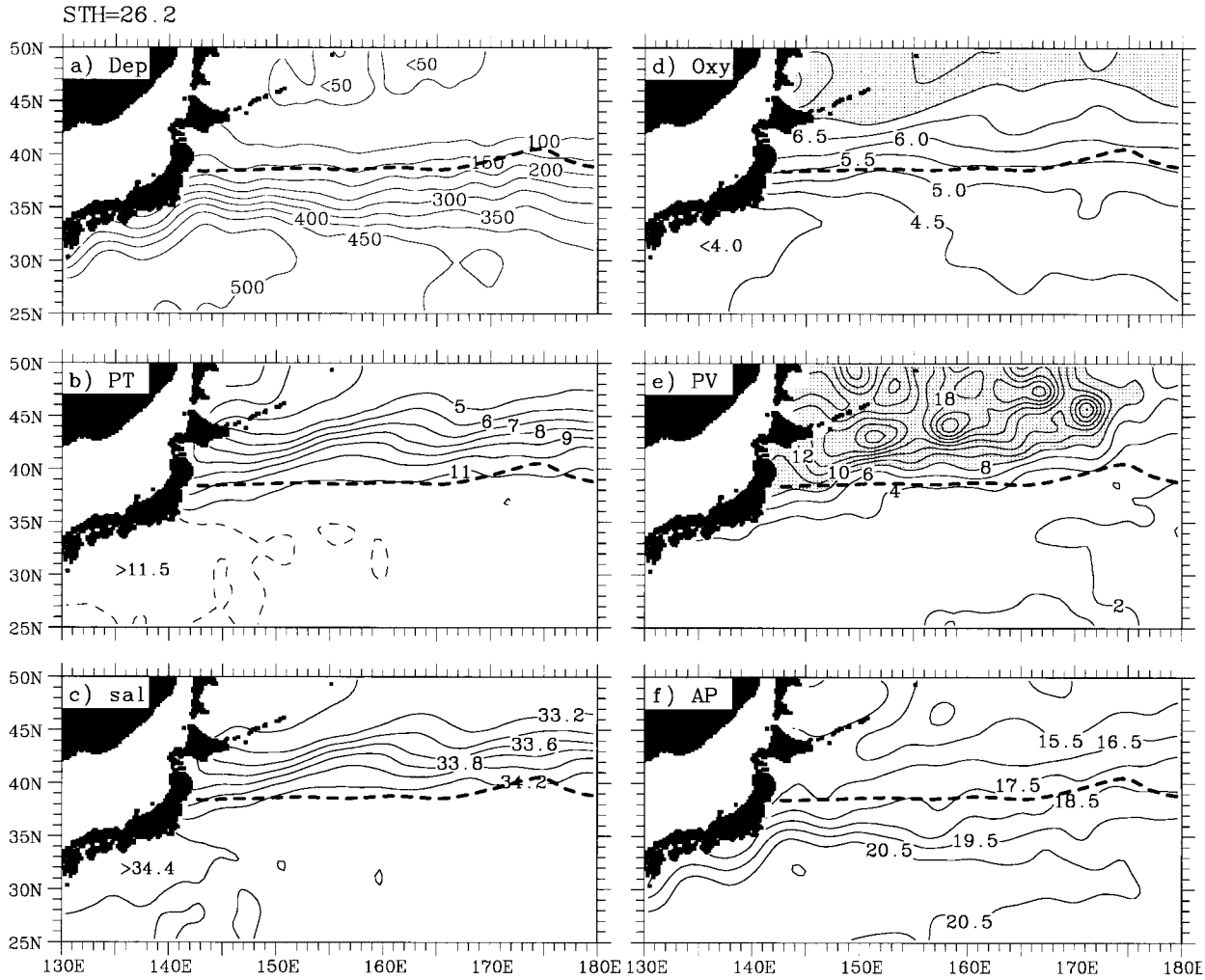

FIG. 5. Distributions of (a) depth (m), (b) potential temperature (°C), (c) salinity (psu), (d) concentration of dissolved oxygen (ml l^{-1}), (e) potential vorticity (10^{-10} m^{-1} s^{-1}), and (f) acceleration potential (m^2 s^{-2}) on 26.2 σ_θ surface. Areas with $O_2 > 7.0$ ml l^{-1} or PV $> 8.0 \times 10^{-10}$ m^{-1} s^{-1} are shaded. The heavy dashed lines indicate the outcropping of this density in Feb from the Levitus (1994) climatology.

Oyashio Front, where potential temperature and salinity gradients are large (Figs. 5b,c), but water density remains rather uniform across the Oyashio Front near the surface.

The concentration of dissolved oxygen increases steadily toward the north (Fig. 5d), with its maximum exceeding 7.5 ml l^{-1} in the northwest. Consonant with this elevated oxygen level is a broad region of high potential vorticity ($>10 \times 10^{-10}$ m^{-1} s^{-1}) in the outcrop zone (north of 38°–40°N), where potential vorticity among several other properties is reset directly by surface forcing. Potential vorticity is rather homogeneous ($\sim 3.0 \times 10^{-10}$ m^{-1} s^{-1}) in the KERG, roughly south of the line from 35°N, 140°E to 43°N, 180°, as has been reported by earlier observations (e.g., Keffer 1985; Talley 1988). The low potential vorticity ($<2 \times 10^{-10}$ m^{-1} s^{-1}) near the international dateline is likely due to the North Pacific central mode water (Suga et al. 1997).

The presence of the Kuroshio and its extension (Fig. 5f) is identical with high potential temperature (>11.5°C), high salinity (>34.4 psu), low oxygen (<4.0 ml l^{-1}), and low potential vorticity ($<4.0 \times 10^{-10}$ m^{-1} s^{-1}) extending eastward from the coast of Japan. The Oyashio is apparent in the acceleration potential map, but there is no significant property core that can be related to this narrow current, reflecting the strong influence of direct ventilation on this density.

b. σ_θ = 26.8

We chose $\sigma_\theta = 26.8$ because it lies near the North Pacific Intermediate Water (NPIW: Reid 1965). NPIW, known as a salinity minimum centered at 26.7–26.9 σ_θ, is formed in the western North Pacific and spreads over the entire basin via large-scale circulations (Talley 1993). In coherence with the formation of NPIW, the 26.8 σ_θ surface has its shallowest ($D < 200$ m), coldest ($T < 2.0$°C), freshest ($S < 33.6$ psu), and newest (O_2

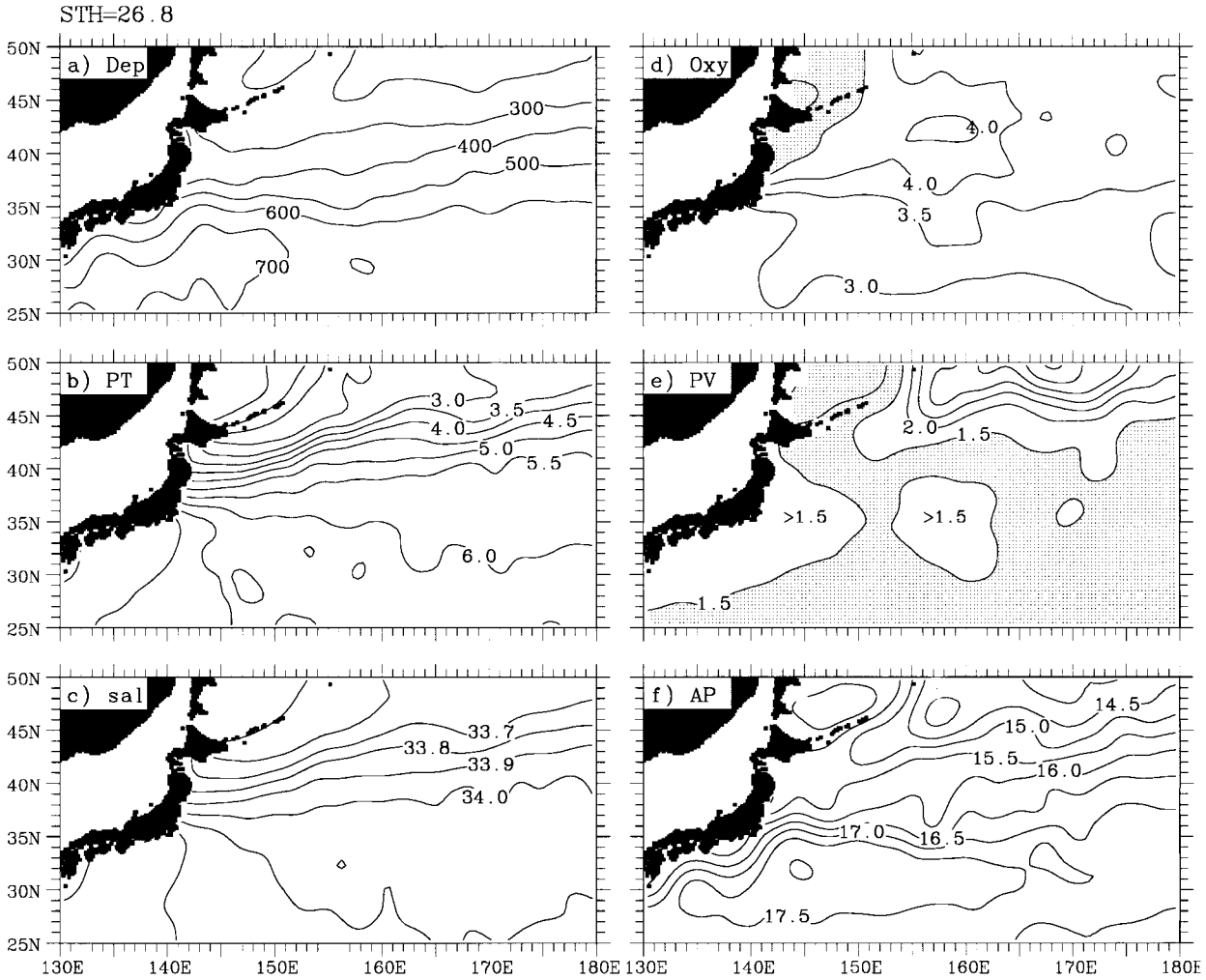

FIG. 6. As in Fig. 5 except on the 26.8 σ_θ surface, areas with $O_2 > 4.5$ ml l^{-1} or PV $< 1.5 \times 10^{-10}$ m^{-1} s^{-1} shaded.

> 4.5 ml l^{-1}) extremes in the Okhotsk Sea and along the coast of the Kuril Islands (Figs. 6a–d). These properties change dramatically toward the southeast in the MWR, approaching a relatively homogeneous state of $D \sim 700$ m, $\theta \sim 6$°C, $S \sim 34.1$ psu, and $O_2 \sim 3.0$ ml l^{-1} south of the Kuroshio Extension.

Potential vorticity around NPIW has been derived and discussed by a variety of investigators (e.g., Talley 1988, 1993; Yasuda 1997). Here, we see a potential vorticity minimum ($<1.0 \times 10^{-10}$ m^{-1} s^{-1}) in the Okhotsk Sea (Fig. 6e), in contrast with a potential vorticity maximum ($>3.0 \times 10^{-10}$ m^{-1} s^{-1}) to the east. Between these two extremes, water with typical potential vorticity of 1.5×10^{-10} m^{-1} s^{-1} extends southward along the coast of the Kuril Islands and Hokkaido and spreads over much of the subtropical region studied. In the light of ''unventilated'' theory (Rhines and Young 1982), this uniform potential vorticity is not surprising, and has been interpreted as evidence that a convective (density driven) source of NPIW is unlikely in the open subtropical Pacific (Talley 1993). Its connection with the potential vorticity minimum in the Okhotsk Sea lends a support for Yasuda's (1997) hypothesis that the origin of NPIW is the Okhotsk Sea mode water.

Two local maxima of potential vorticity ($>1.5 \times 10^{-10}$ m^{-1} s^{-1}) appear in the subtropical region (Fig. 6e). One hugs the coast of Japan, with its high value extending eastward along 35°N, and the other is situated in the vicinity of the Shatsky Rise centered at about 35°N, 158°E. The former, also evident in the previous analyses (e.g., Talley 1993), apparently reflects the influence of the Kuroshio (Fig. 6f). The latter has not been previously reported. The mechanisms responsible for its existence are not presently known, but we speculate that bottom topography might play a role, given its geographical coincidence with the Shatsky Rise.

c. $\sigma_\theta = 27.2$

The 27.2 σ_θ surface is where the Antarctic Intermediate Water (AAIW) spreads over the North Pacific

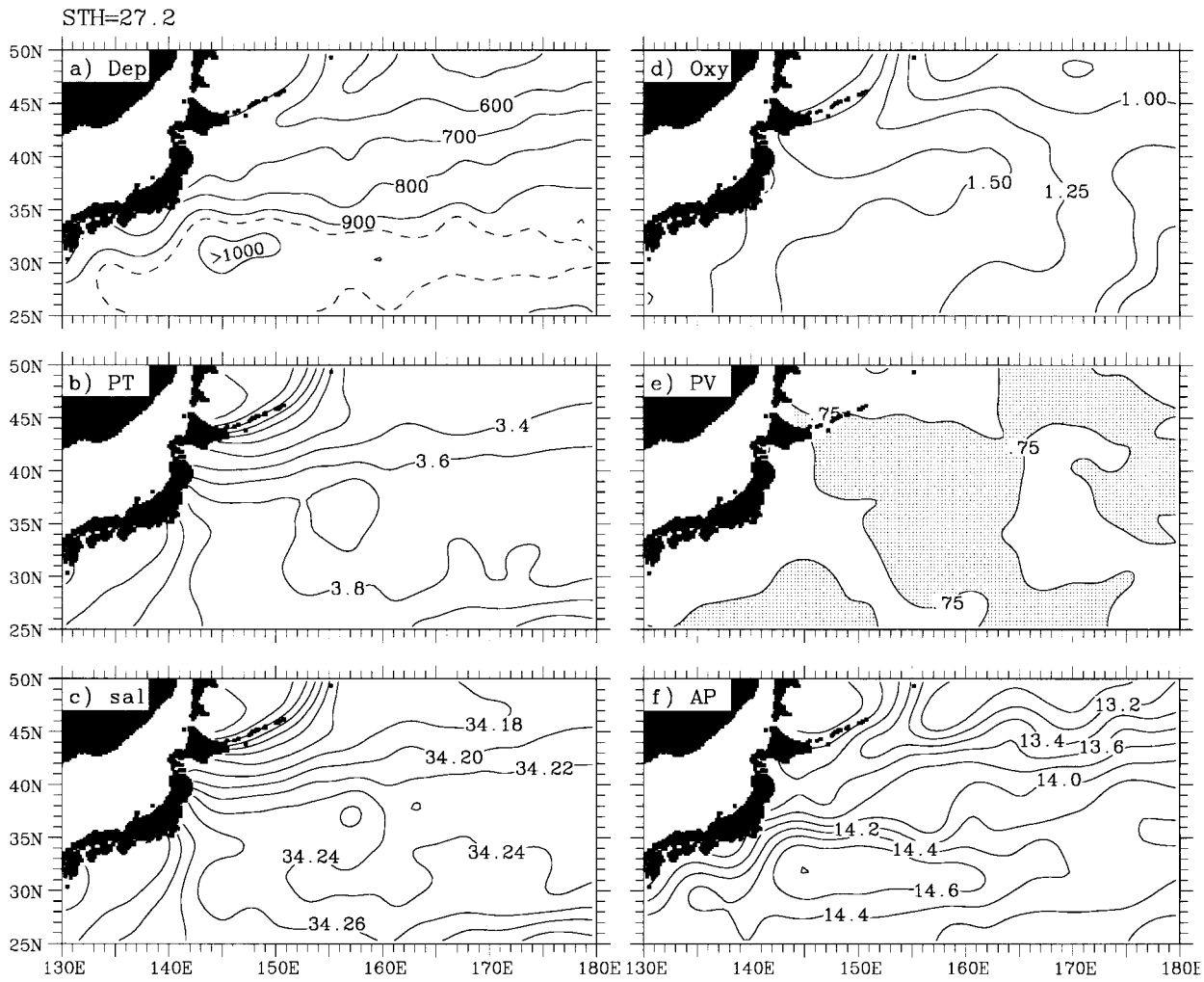

FIG. 7. As in Fig. 5 except on the 27.2 σ_θ surface, area with PV $<0.75 \times 10^{-10}$ m^{-1} s^{-1} shaded.

(Reid 1965). Although the spreading of AAIW is beyond the interest of this study, maps of property distribution at this density may be useful for further investigation of the water exchange between the subtropical and subpolar gyres. This density, lying between 500 and 1000 m depths (Fig. 7), is just above the oxygen minimum originated from the subpolar gyre (Reid 1965; Wijffels et al. 1998). The strong influence of the subpolar source can be identified by the low oxygen level (<1.4 ml l^{-1}) extending southwestward along the Kuril Islands and Hokkaido. A relatively high oxygen level (>1.4 ml l^{-1}) is seen in the Kuroshio and its extension where the influence of the subtropical source seems to be dominant.

6. Sectional distributions

a. Along 145°E

Section 145°E crosses the Kuroshio Extension and Oyashio Front at their very beginning. Along the section properties undergo a rapid change at about 35°N, indicative of a strong (>25 cm s^{-1}) zonal flow (i.e., the Kuroshio Extension) toward the east (Fig. 8). The Oyashio Front is underdeveloped at this longitude, so only a weak eastward flow is seen at 41°–42°N.

In general properties are horizontally homogeneous south of the Kuroshio Extension and change dramatically to the north on the shallow isopycnal surfaces ($\sigma_\theta \leq 26.2$), as already noted in section 5a. To the south of the Kuroshio Extension, the seasonal thermocline overrides a thick layer of high salinity (>34.7 psu) and low potential vorticity ($<1.5 \times 10^{-10}$ m^{-1} s^{-1}), commonly known as the subtropical mode water (STMW) formed by wintertime deep convection as a result of strong surface cooling (Hanawa 1987). A potential vorticity maximum ($>3.0 \times 10^{-10}$ m^{-1} s^{-1}) layer with oxygen level >3.0 ml l^{-1} appears underneath the STMW, stretching southward from about 36° to 32°N along isopycnal surfaces centered at $\sigma_\theta = 26.1$. This potential vorticity maximum layer is an expression of the main thermocline

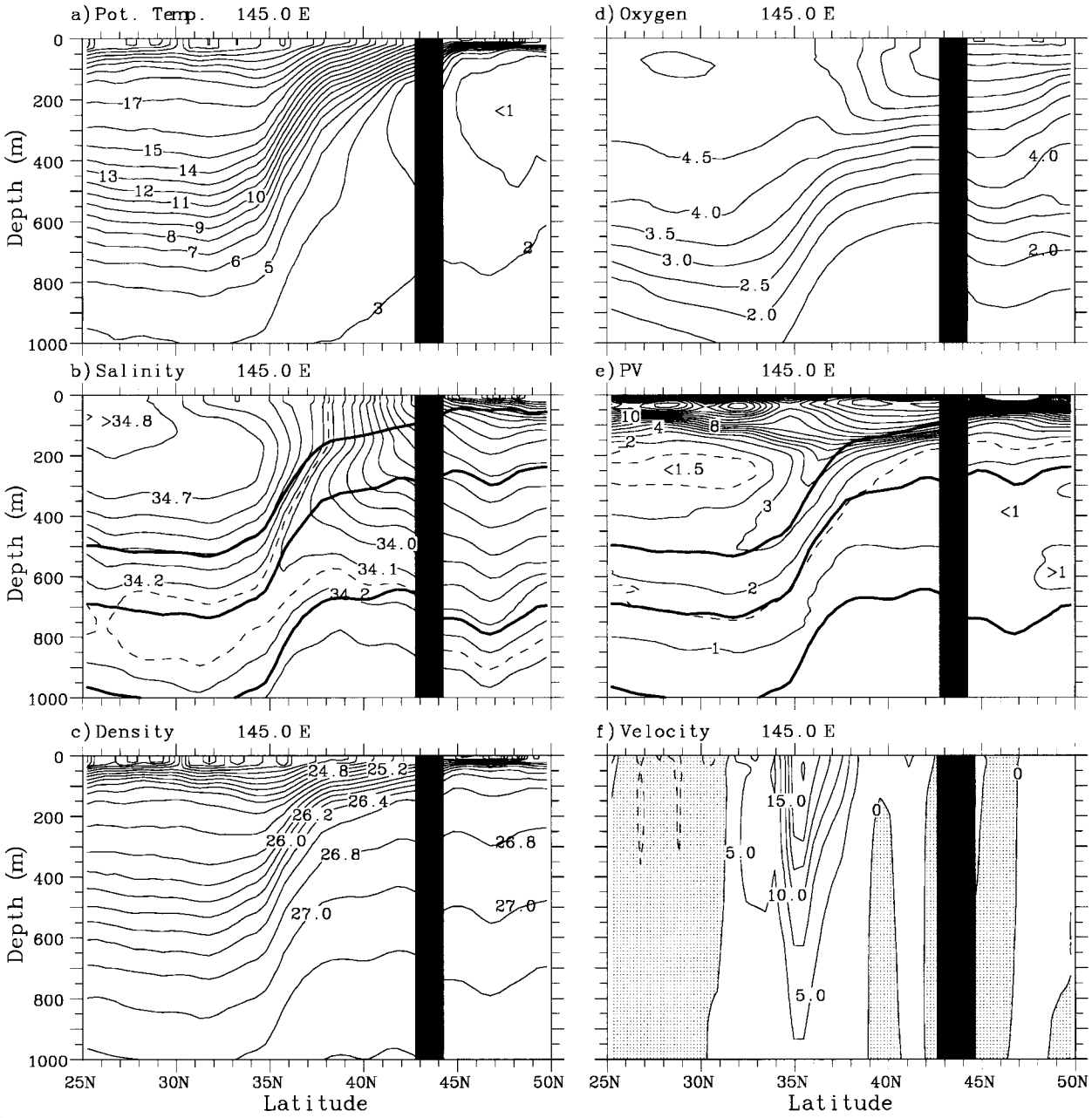

FIG. 8. Vertical sections of (a) potential temperature (°C), (b) salinity (psu), (c) potential density (kg m^{-3}), (d) dissolved oxygen concentration (ml l^{-1}), (e) potential vorticity (10^{-10} m^{-1} s^{-1}), and (f) geostrophic velocity (cm s^{-1}) relative to 2000 dbar along 145°E. Positive velocities are eastward and negative values are shaded. Thick lines in (b) and (e) indicate 26.2, 26.8, and 27.2 σ_θ surfaces, and dashed lines show additional contours of 34.15 psu in (b) and 1.5 × 10^{-10} m^{-1} s^{-1} in (e).

(Talley 1988), whose origins are not well known. The NPIW (around 26.8 σ_θ surface) marks the bottom of recently ventilated thermocline water of low salinity (<34.1 psu) and high oxygen (about 3.0 ml l^{-1}). Below that depth, water properties are conserved following isopycnal flow.

There is a discontinuity of properties across the Kuril Islands, with lower salinity and higher oxygen on the northern side. This discontinuity of properties could be due to the presence of the Kuril Islands that blocks deep-sea water exchange between the two sides. In the Okhotsk Sea, water has a potential temperature minimum (<1°C) centered at about 200 m. Low salinity is responsible for a stable density stratification around that depth. Below 200 m there is a broad layer of homogenous potential vorticity at 0.5–1.0 (×10^{-10} m^{-1} s^{-1}).

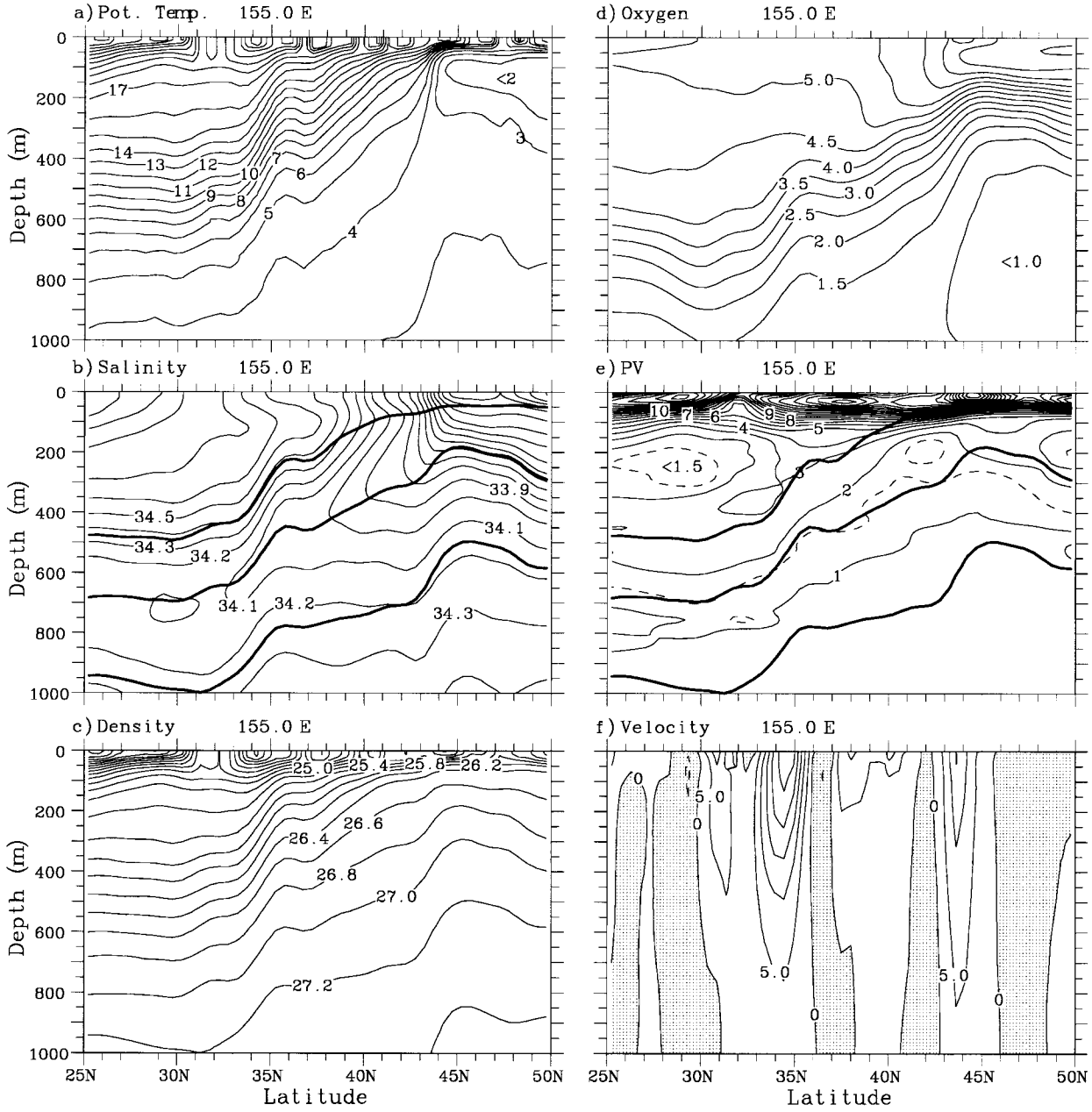

FIG. 9. As in Fig. 8 except along 155°E.

Potential vorticity in its upper portion is significantly lower in the Okhotsk Sea than it is to the south, and this trend is reversed in its lower portion (Fig. 8).

b. Along 155°E

The Oyashio Front becomes well developed at 155°E with its maximum speed exceeding 15 cm s^{-1} around 43°N (Fig. 9). The Kuroshio Extension remains very much the same as described above. Two fronts are therefore defined in the density field, one at about 34°N and the other at about 43°N. Density between these two fronts is relatively homogeneous, giving a typical step-like distribution. As already noticed in section 4, this double-front structure does not have a strong signature near the surface, but seems to be well defined at depths in and below the thermocline.

Figures 8 and 9 reveal the existence of a weak westward flow immediately to the north of the Kuroshio Extension at 36°–40°N. This westward return flow seems to be a robust phenomenon at longitudes west of 160°E. Similar results were also observed from direct current measurements (e.g., Schmitz et al. 1987; Joyce and Schmitz 1988) and surface drifters (Maximenko et

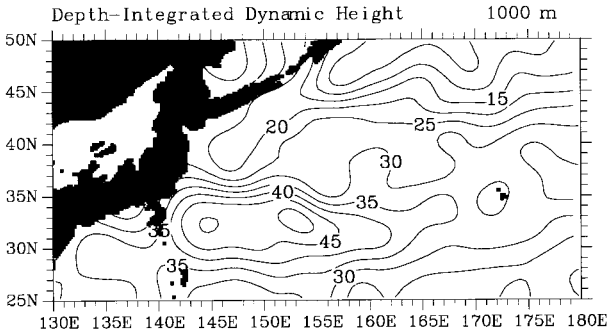

FIG. 10. Depth-integrated (1000–2000 m) dynamic height (m^2) relative to 2000 dbar. Contour intervals are 5 m^2. The value of 265 m^2 has been subtracted before plotting.

al. 1998). We have indicated that such a westward return flow is required by the Sverdrup dynamics (section 3). Another hypothesis is associated with eddy-driven recirculation gyres to the north of an eastward-flowing jet (e.g., Jayne et al. 1996).

7. Middepth circulation

To examine the structure of the KOS at middepths, we include a map of depth-integrated dynamic height from 2000 to 1000 m (Fig. 10). Although the assumption of a level of no motion at 2000 dbar misses the barotropic component (e.g., Joyce and Schmitz 1988), the strong signature of the Kuroshio Extension and the Oyashio Front is still evident within this depth range. The relative transport associated with the Oyashio Front (2.3 Sv at 160°E) is of comparable strength with that of the Kuroshio Extension (3.3 Sv at 153°E). But, the latter seems to be dominated by the eastward flow component on the northern side of the KERG centered at 145°–155°E. Farther to the east, contours of depth-integrated dynamic height turn northeastward, leaving the area dominated by a weak westward flow south of 35°N. Compared with its shallower water counterpart (Figs. 3b and 4a–c), there is clearly a poleward migration of the east–west axis, defined as a meridional maximum of dynamic height, at middepths of the subtropical gyre (Reid and Arthur 1975; Reid and Mantyla 1978). This does not seem to be the case near the western boundary (west of 160°E), presumably as a result of coastline orientation, nonlinear effect, and bottom topography (Hurlburt et al. 1996).

A prominent feature of the North Pacific at middepths is a well-defined vertical oxygen minimum that appears weakly at 27.2 and clearly at 27.4 σ_θ (Reid 1965; Reid and Mantyla 1978). We choose 27.4 σ_θ to infer the circulation and water mass distribution around this oxygen minimum (Figs. 11a–f). The 27.4 σ_θ surface, according to Reid and Mantyla, outcrops near 60°S in southern winter, and beyond that latitude it lies too deep for any substantial renewal from above by vertical processes. As a result, the pattern of oxygen over the Pacific is dominated by high values entering from the south and low values found in the north (Reid and Mantyla 1978).

The depth of 27.4 σ_θ surface varies between 850 and 1250 m in the western North Pacific (Fig. 11a). Its depth variations reflect the sort of density field one would expect from the map of geostrophic flow, including the southward intrusion of the Oyashio along the coast of the Kuril Islands and the KERG centered at 140°–155°E along 32°N (Fig. 11f). A tongue of low oxygen level (<0.8 ml l^{-1}) is seen extending southwestward from the international dateline south of 35°N (Fig. 11d). Another pathway of low oxygen level is associated with the southward intrusion of the Oyashio along the Kuril Islands. The signature of oxygen minimum disappears off Honshu, presumably as a result of mixing with the warm, salty, and oxygen-rich subtropical waters (Figs. 11b–d).

High oxygen is seen extending northeastward from about 38°N, 160°E (Fig. 11d). It appears that the northeastward flow of the subtropical waters separated from the Kuroshio Extension near the Shatsky Rise (Fig. 11f) can account for this pattern of oxygen. Potential vorticity is particularly uniform along this density surface, ranging between 0.4 and 0.5 ($\times 10^{-10}$ m^{-1} s^{-1}) for most of the region studied (Fig. 11e). Only within the Okhotsk Sea and near the coast of Hokkaido and Tohoku does it exceed 0.5×10^{-10} m^{-1} s^{-1}.

The present result fits the middepth circulation diagram of the Pacific provided by Reid and Mantyla (1978). According to this earlier study, oxygen-rich water enters in the west from the South Pacific and passes across the equator and northward with the western boundary current. From there two eastward flowing branches carry the newer water across the North Pacific, one from about 35°N in the west to about 45°N in the east and the other from about 20°N in the western and central areas to about 30°N in the east. The former is evident as a northeastward extension of high oxygen from about 38°N at 160°E (Fig. 11d). Reid and Mantyla also noted that there are two adjacent westward flows extending as wedges of low oxygen between the branches carrying the new waters. The northern one corresponds to the tonguelike spreading of low oxygen south of 35°N (Fig. 11d).

8. Summary

Mean circulation and water mass distributions are investigated using historical data in the western North Pacific. In contrast with previous climatological analyses (e.g., Levitus 1982, 1994), we average the data along isopycnal instead of pressure surfaces in a 0.5° $\times$ 0.5° grid with *e*-folding smoothing scales less than 100 km in the upper 1000 m. This approach yields improved results, and better resolves the Kuroshio/Oyashio system.

First of all, the present analysis demonstrates many small-scale semipermanent features of the region in-

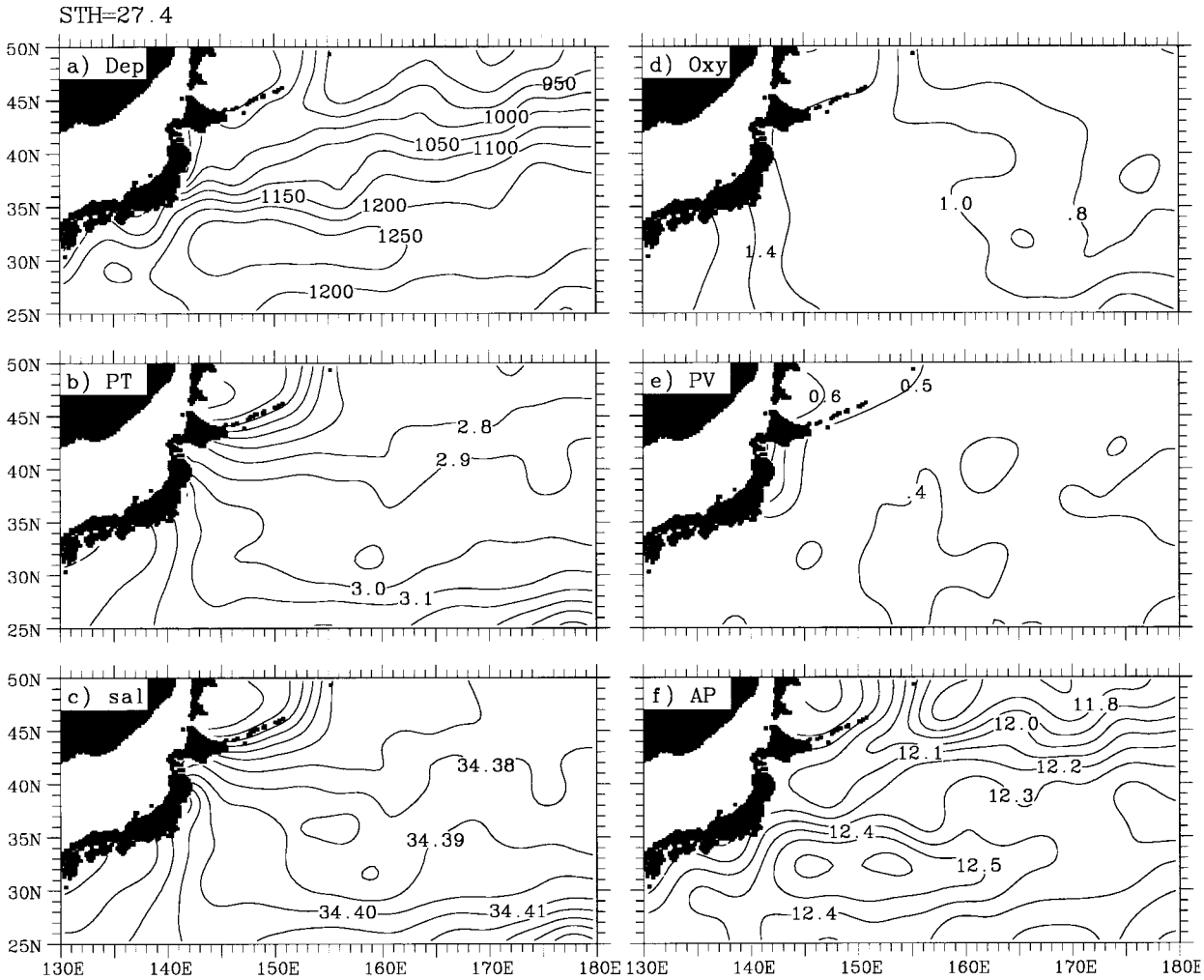

FIG. 11. Distributions of (a) depth (m), (b) potential temperature (°C), (c) salinity (psu), (d) concentration of dissolved oxygen (ml l^{-1}), (e) potential vorticity (10^{-10} m^{-1} s^{-1}), and (f) acceleration potential (m^2 s^{-2}) on 27.4 σ_θ surface.

cluding the southward deflection of the Kuroshio south of Honshu, two anticyclonic meanders of the Kuroshio Extension near 144° and 150°E, and the bifurcation of the Kuroshio Extension near Shatsky Rise. Most strikingly, the southward intrusion of the Oyashio occurs as far south as 36°–38°N off the Japanese coast and extends as deep as middepths. While these results are already known from synoptic measurements, they have not been represented heretofore in a climatology.

The time-averaged structure of the KOS is depth dependent. At depths of the thermocline, it exhibits a well-defined double-front structure with the Kuroshio Extension flowing eastward along 34°–36°N and the Oyashio Front extending northeastward from 36°–38°N near the coast to 40°–45°N offshore. This structure does not have a strong signature near the surface. Water density remains rather uniform across the Oyashio Front in the surface layer, despite large temperature and salinity gradients.

Both the Kuroshio Extension and Oyashio Front have a significant deep (1000 m) component, as we have already known from direct current measurements (e.g., Joyce and Schmitz 1988), but the former seems to be dominated by a strong eddy feature associated with the KERG centered at 30°–32°N, 140°–155°E at middepths. In the ocean interior (east of 160°E), the east–west axis of the subtropical gyre defined as a meridional maximum of dynamic height tends to shift northward from about 30°N near the surface to about 35°N at middepths, reflecting the poleward contraction on denser surfaces (Reid and Arthur 1975). By contrast, the east–west axis of the KERG (west of 160°E) does not vary with depth in any significant ways, presumably due to the strong influence of bottom topography.

An important aspect of the regional dynamics is that water from the subpolar gyre crosses the zero zonally integrated wind-stress-curl line into the subtropical gyre at the western boundary (e.g., Kawai 1972; Sekine 1988;

Hurlburt et al. 1996), and this southward intrusion of the Oyashio is clearly demonstrated in our climatology. At least part of the Oyashio overshoots the latitude required by the Sverdrup constraint by more than 5°. In the ocean interior, water separated from the Kuroshio Extension tends to feed into the Oyashio Front to satisfy the Sverdrup constraint. As such, the zero meridional transport integrated from the western boundary to 180° occurs at about 44°N, coinciding with the zero wind-stress-curl line.

A narrow westward flow is identified from dynamic topography field between the Kuroshio Extension and Oyashio Front. In contrast with previous observations (e.g., Schmitz et al. 1987; Joyce and Schmitz 1988; Maximenko et al. 1998), we find that this westward flow extends down to at least the middepths in a broad longitude band from the Japanese coast to 160°E. The mechanism responsible for driving this westward flow is not presently understood. Sverdrup transport with a local minimum along 36°–40°N gives a possible explanation. Another hypothesis is associated with the eddy-driven flow (Jayne et al. 1996).

Finally, we note that in the interest of uniformity of the database, the present analysis was restricted to the upper 2000 m alone. Since the KOS has a significant barotropic component, the selection of a depth of no-motion at 2000 m might underestimate its intensity. Despite this weakness, this study has provided probably the most accurate three-dimensional, time-averaged picture up to date of the KOS east of Japan. This picture should be useful for the design and analysis of future observations and simulations as well.

Acknowledgments. This research was supported by the Frontier Research System for Global Change through its sponsorship of the International Pacific Research Center. We thank J. McCreary, T. Yamagata, K. Hanawa, and S.-P. Xie for valuable discussions throughout this study. Thanks are also extended to N. Hogg, A. M. Macdonald, T. Suga, and R. G. Curry for useful communications on the present topic and to L. Talley and two anonymous reviewers for thoughtful comments on the earlier manuscript.

APPENDIX

Error Analysis

The observations used in preparing the present dataset were collected in various seasons of different years. Since the MWR is a region of strong variations, ranging from synoptic to interdecadal timescales, the uncertainty in the mean fields of water properties is generally large. A measure of this uncertainty is afforded by the standard deviation information. At depths around the main thermocline (Fig. A1), typical potential temperature, salinity, and oxygen concentration standard deviations (defined as the spatial averages over the domain) are 0.75°C, 0.12 psu, and 0.42 ml l^{-1}, respectively. The spatial distribution of the standard deviations shows larger uncertainties in the latitude band of 35°–45°N, roughly coinciding with the property front shown in Fig. 5.

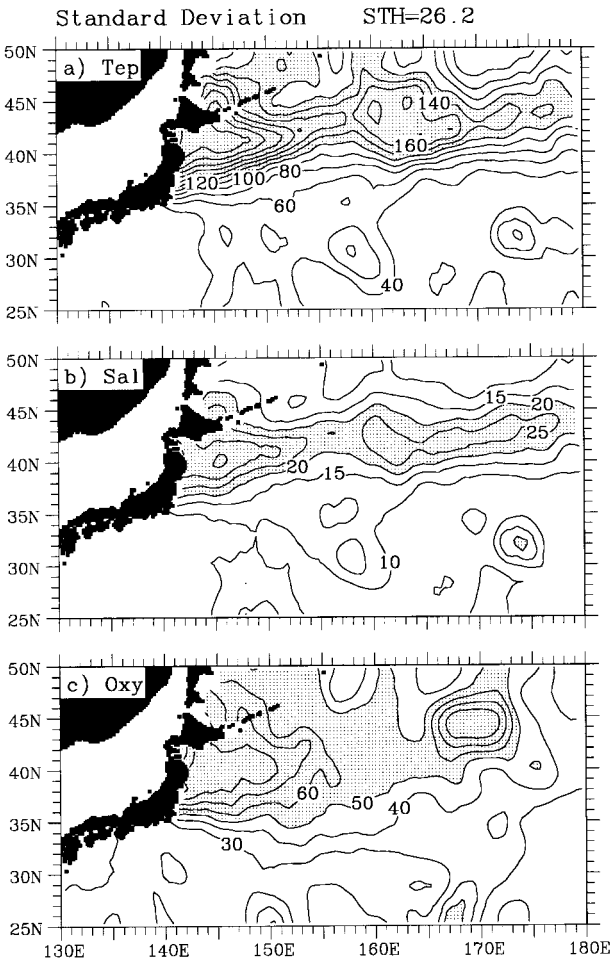

FIG. A1. Standard deviations (STD) of (a) potential temperature in 0.01°C, (b) salinity in 0.01 psu, and (c) dissolved oxygen concentration in 0.01 ml l^{-1} on the 26.2 σ_θ surface, areas with STD potential temperature >1.2°C, STD salinity >0.2 psu, or STD oxygen >0.5 ml l^{-1} shaded.

Standard deviations decrease with depth, being of the order of 0.48°C for potential temperature, 0.07 psu for salinity, and 0.48 ml l^{-1} for oxygen concentration on the 26.8 σ_θ surface (Fig. A2). The maximum potential temperature and salinity standard deviations are seen in the confluence area between the Kuroshio and Oyashio east of Japan. The standard deviation of oxygen concentration is also large near the cost of Tohoku and Hokkaido, but its maximum seems to extend somewhat northward. This pattern of standard deviations remains nearly unchanged before reaching σ_θ = 27.2. On σ_θ = 27.2, typical standard deviations of potential temperature, salinity, and oxygen concentration are 0.2°C, 0.03 psu, and 0.25 ml l^{-1}, respectively. At depths below σ_θ = 27.2, the spatial distribution of standard deviations

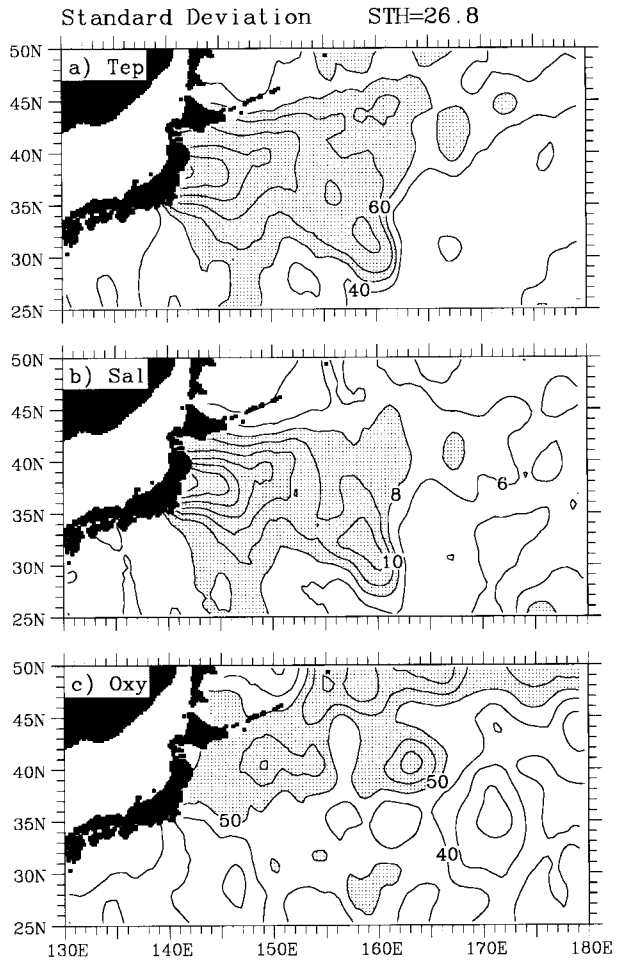

FIG. A2. As in Fig. A1 except on 26.8 σ_θ surface, areas with STD potential temperature >0.5°C, STD salinity >0.08 psu, or STD oxygen >0.5 ml l^{-1} shaded.

is relatively uniform (not shown), and their typical values fall below 0.15°C, 0.02 psu, and 0.18 ml l^{-1}, respectively, for potential temperature, salinity, and oxygen concentration at 1600 m. The estimates of standard deviations were based in most cases on ensembles of more than 10 measurements, so the standard errors of the mean property fields are typically 3–4 times (the square root of the number of measurements) smaller than the standard deviations described above. In the case that the number of measurements is as large as several hundred, the standard errors are even smaller. In addition to time variations, the uncertainty in the mean fields could also be due to the bad quality of the data. Since most of the observations used for this study were made at conventional standard depths, the interpolated values on isopycnal surfaces are subject to a large uncertainty. Although there is no easy way to quantify this uncertainty, its effect on the mean field is expected to be much reduced by the combined use of observations from different seasons of different years. So, we feel that the time-averaged structure of the KOS described in this study should be representative.

REFERENCES

Gouriou, Y., and J. Toole, 1993: Mean circulation of the upper layers of the western equatorial Pacific Ocean. *J. Geophys. Res.,* **98,** 22 495–22 520.

Hall, M. M., 1989: Velocity and transport structure of the Kuroshio Extension at 35°N, 152°E. *J. Geophys. Res.,* **94,** 14 445–14 459.

Hanawa, K., 1987: Interannual variations of the wintertime outcrop area of subtropical mode water in the western North Pacific Ocean. *Atmos.–Ocean,* **25,** 358–374.

Hellerman, S., and M. Rosenstein, 1983: Normal monthly wind stress over the world ocean with error estimates. *J. Phys. Oceanogr.,* **13,** 1093–1104.

Hurlburt, H. E., A. J. Wallcraft, W. J. Schmitz, P. J. Hogan, and E. J. Metzger, 1996: Dynamics of the Kuroshio/Oyashio current system using eddy-resolving models of the North Pacific Ocean. *J. Geophys. Res.,* **101,** 941–976.

Jayne, S., N. Hogg, and P. Malanotte-Rizzoli, 1996: Recirculation gyres forced by a beta-plane jet. *J. Phys. Oceanogr.,* **26,** 492–504.

Joyce, T. M., 1987: Hydrographic sections across the Kuroshio extension at 165°E and 175°W. *Deep-Sea Res.,* **34,** 1331–1352.

——, and W. J. Schmitz, 1988: Zonal velocity structure and transport in the Kuroshio Extension. *J. Phys. Oceanogr.,* **18,** 1484–1494.

Kawai, H., 1972: Hydrography of the Kuroshio Extension. *Kuroshio: Physical Aspects of the Japan Current,* H. Stommel and K. Yoshida, Eds., University of Washington Press, 235–354.

Keffer, T., 1985: The ventilation of the world's oceans: Maps of the potential vorticity field. *J. Phys. Oceanogr.,* **15,** 509–523.

Levitus, S., 1982: *Climatological Atlas of the World Oceans.* NOAA Prof. Paper. No. 13, U.S. Govt Printing Office, Washington, DC, 173 pp.

——, 1994: *World Ocean Atlas 1994.* Vol. 13, NOAA Atlas NESDIS, CD–ROM.

Lu, P., J. P. McCreary, and B. A. Klinger, 1998: Meridional circulation cells and the source waters of the Pacific Equatorial Undercurrent. *J. Phys. Oceanogr.,* **28,** 62–84.

Macdonald, A. M., T. Suga, and R. G. Curry, 2001: An isopycnally averaged North Pacific climatology. *J. Atmos. Oceanic Technol.,* **18,** 394–420.

Maximenko, N., G. Panteleev, P. Niiler, and T. Yamagata, 1998: Near-surface circulation in the northwestern Pacific as derived from Lagrangian drifters. *Proc. Int. Symp. TRIANGLE'98,* Kyoto, Japan, Japan Marine Science and Technology Center, Frontier Research System for Global Change, and International Pacific Research Center, 81–90.

McCreary, J. P., and P. Lu, 1994: On the interaction between the subtropical and the equatorial oceans: The subtropical cell. *J. Phys. Oceanogr.,* **24,** 466–497.

Miller, A. J., D. R. Cayan, and W. B. White, 1998: A westward-intensified decadal change in the North Pacific thermocline and gyre-scale circulation. *J. Climate,* **11,** 3112–3127.

Mitsudera, H., Y. Yoshikawa, B. Taguchi, and H. Nakamura, 1998: Simulation of the Kuroshio and Oyashio system: Preliminary results. *Proc. Int. Symp. TRIANGLE'98,* Kyoto, Japan, Japan Marine Science and Technology Center, Frontier Research System for Global Change, and International Pacific Research Center, 55–64.

Mizuno, K., and W. B. White, 1983: Annual and interannual variability in the Kuroshio current system. *J. Phys. Oceanogr.,* **13,** 1847–1867.

Nakamura, H. G., G. Lin, and T. Yamagata, 1997: Decadal climate variability in the North Pacific during the recent decades. *Bull. Amer. Meteor. Soc.,* **78,** 2215–2225.

Niiler, P. P., W. J. Schmitz, and D. K. Lee, 1985: Geostrophic mass

transport in the high eddy energy regions of the Kuroshio and Gulf Stream. *J. Phys. Oceanogr.,* **15,** 825–843.
Nitani, H., 1972: Beginning of the Kuroshio. *Kuroshio: Physical Aspects of the Japan Current,* H. Stommel and K. Yoshida, Eds., University of Washington Press, 129–163.
Qiu, B., 1995: Variability and energetics of the Kuroshio Extension and its recirculation gyre from the first two-year TOPEX data. *J. Phys. Oceanogr.,* **25,** 1827–1842.
——, 1999: Seasonal eddy field modulation of the North Pacific subtropical countercurrent: TOPEX/Poseidon observations and theory. *J. Phys. Oceanogr.,* **29,** 2471–2486.
——, and K. A. Kelly, 1993: Upper-ocean heat balance in the Kuroshio Extension region. *J. Phys. Oceanogr.,* **23,** 2027–2041.
——, ——,and T. M. Joyce, 1991: Mean flow and variability in the Kuroshio Extension from Geosat altimetry data. *J. Geophys. Res.,* **96,** 18 491–18 507.
Qu, T., H. Mitsudera, and T. Yamagata, 1998: On the western boundary currents in the Philippine Sea. *J. Geophys. Res.,* **103,** 7537–7548.
——, ——, and ——,1999: A climatology of the circulation and water mass distribution near the Philippine coast. *J. Phys. Oceanogr.,* **29,** 1488–1505.
Reid, J. L., 1965: *Intermediate Waters of the Pacific Ocean.* The Johns Hopkins Oceanographic Studies, No. 2, 85 pp.
——, and R. S. Arthur, 1975: Interpretation of maps of geopotential anomaly for the deep Pacific Ocean. *J. Mar. Res.,* **33** (Suppl.), 37–52.
——, and A. W. Mantyla, 1978: On the mid-depth circulation of the North Pacific Ocean. *J. Phys. Oceanogr.,* **8,** 946–951.
Rhines, P. B., and W. R. Young, 1982: A theory of the wind-driven circulation. I. Mid-ocean gyres. *J. Mar. Res.,* **40** (Suppl.), 559–596.
Schmitz, W. J., P. P. Niiler, and C. J. Koblinsky, 1987: Two-year moored instrument results along 152°E. *J. Geophys. Res.,* **92,** 10 826–10 834.
Sekine, Y., 1988: Anomalous southward intrusion of the Oyashio east of Japan. Pt. I: Influence of the seasonal and interannual variations in the wind stress over the North Pacific. *J. Geophys. Res.,* **93,** 2247–2255.
Suga, T., and K. Hanawa, 1990: The mixed-layer climatology in the northwestern part of the North Pacific subtropical gyre and the formation area of Subtropical Mode Water. *J. Mar. Res.,* **48,** 543–566.
——, Y. Takei, and K. Hanawa, 1997: Thermostad distribution in the North Pacific subtropical gyre: The Central Mode Water and the Subtropical Mode Water. *J. Phys. Oceanogr.,* **27,** 140–152.
Talley, L. D., 1988: Potential vorticity distribution in the North Pacific. *J. Phys. Oceanogr.,* **18,** 89–106.
——, 1993: Distribution and formation of North Pacific Intermediate Water. *J. Phys. Oceanogr.,* **23,** 517–537.
Wijffels, S. E., M. M. Hall, T. Joyce, D. Torres, P. Hacker, and E. Firing, 1998: Multiple deep gyres of the western North Pacific: A WOCE section along 149°E. *J. Geophys. Res.,* **103,** 12 985–13 009.
Xie, S.-P., T. Kunitani, A. Kubokawa, M. Nonaka, and S. Hosoda, 2000: Interdecadal thermocline variability in the North Pacific for 1958–1997: A GCM simulation. *J. Phys. Oceanogr.,* **30,** 2798–2813.
Yasuda, I., 1997: The origin of the North Pacific Intermediate Water. *J. Geophys. Res.,* **102,** 893–909.